ACS Catalysis

Research Article

pubs.acs.org/acscatalysis

Palladium Nanocatalysts Immobilized on Functionalized Resin for the Direct Synthesis of Hydrogen Peroxide from Hydrogen and Oxygen

Jongmin Kim,[†,§] Young-Min Chung,[‡,§] Sung-Min Kang,[†] Chang-Hyung Choi,[†] Bo-Yeol Kim,[†] Yong-Tak Kwon,[‡] Tae Jin Kim,[‡] Seung-Hoon Oh,[‡] and Chang-Soo Lee*[,†]

[†]Department of Chemical Engineering, Chungnam National University, Yuseong-gu, Daejeon 305-764, Republic of Korea

[‡]Catalyst Lab, Catalyst & Process R&D Centre, SK innovation, Yuseong-gu, Daejeon 305-712, Republic of Korea

Supporting Information

ABSTRACT: The direct synthesis of hydrogen peroxide (DSHP) from H_2 and O_2 is conceptually the most ideal and straightforward reaction for producing H_2O_2 in industry. However, precisely tailored catalysts are still in progress for large scale production. Here, we report highly efficient and industrially relevant catalysts for the direct synthesis of H_2O_2 from H_2 and O_2 prepared by the immobilization of Pd nanocatalysts onto a functionalized resin. The continuous production of 8.9 wt % H_2O_2 and high productivity (180 g of H_2O_2 (g of Pd)$^{-1}$ h^{-1}) is achieved under intrinsically safe and less-corrosive conditions without any loss of activity. We expect this approach is a substantial improvement of nanocatalysts for direct synthesis of hydrogen peroxide from hydrogen and oxygen and will greatly accelerate the industrially relevant process of on site production of hydrogen peroxide soon.

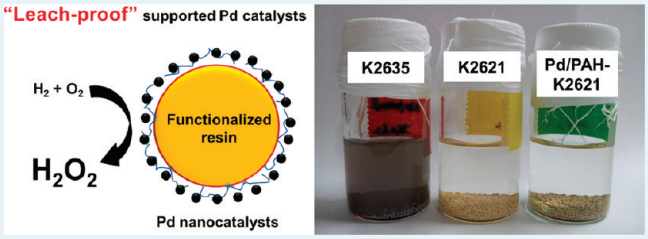

KEYWORDS: *Direct synthesis of hydrogen peroxide, Leach proof, Pd nanoparticles, Immobilization, on site production*

INTRODUCTION

The direct synthesis of hydrogen peroxide (DSHP) from hydrogen and oxygen has drawn attention from its infancy because of the simple reaction scheme involved and because water is the only byproduct. Contrary to the simple reaction scheme, unfortunately, the reaction remains one of the most challenging reactions from a catalysis perspective.[1] The DSHP can be explosive when operated within flammability/explosion limits (mixing ratio of H_2/O_2 in the range from 4% to 94% H_2).[2] On account of these serious problems, the direct process has not yet been put into practice. Thus, in order to be out of the explosive region, the mixtures of H_2 and O_2 should contain less than about 4% H_2. Although continuous efforts are underway to improve catalyst and reactor designs and to optimize process parameters for this reaction,[3−6] both the efficiency of the catalysts and the concomitant intrinsic problems that involve thermodynamic free energies in the reaction pathway remain unsatisfactory.

Recently, research along these lines has been rejuvenated by important contributions from leading research groups. Hutchings and colleagues have focused on Au−Pd bimetallic catalysts,[7−10] while Lunsford et al. have opened a new avenue of catalyst design by introducing supported Pd nanoparticle catalysts.[11] Especially, Fierro's group gives important contributions on the basis of palladium-loaded sulfonic acid polystyrene resin catalysts.[12−15] Huilin et al. has demonstrated the relatively safe DSHP operation in the absence of any acid and halide promoter under the atmosphere pressure.[16] In industrial fields, Evonik Industries (formerly Degussa-Headwaters) have made efforts to implement the DSHP process with their proprietary "phase-controlled" nanoparticle-based catalysts.[17,18] By virtue of these pioneering contributions, expectations for the successful development of the DSHP process are high. From an industrial viewpoint, however, the reaction is still considered an elusive goal. Because the development of the process has been hampered by critical issues such as low selectivity, low productivity of H_2O_2, and corrosion/leaching problems caused by caustic reaction media, it is extremely difficult to meet the industrial target of continuous production of 8−10 wt % H_2O_2 under industrially relevant conditions. These challenges may account for the few commercial implementations of this reaction.

As a preliminary step to achieving the elusive goal of the continuous production of 8−10 wt % H_2O_2, we have previously proposed an efficient catalyst design based on the encapsulation of Pd nanoparticles in polyelectrolyte multilayers (PEMs) constructed on an ion-exchange resin.[19] This approach has shown that the H_2O_2 yield is sufficiently high to meet the industrial target under intrinsically safe and less-corrosive conditions without any loss of activity. However, the amount of Pd nanoparticles near the surface of the catalyst is relatively small because the nanoparticles are intercalated and distributed

Received: February 6, 2012
Revised: April 16, 2012
Published: April 19, 2012

Scheme 1. Formation of Pd Nanocatalysts onto Sulfonated Resin: (a) Pd-DDS Synthesis; (b) Ligand Exchange of Pd-DDS with Water-Soluble MAA; (c) Immobilization of Pd-MAA onto Functionalized Resin

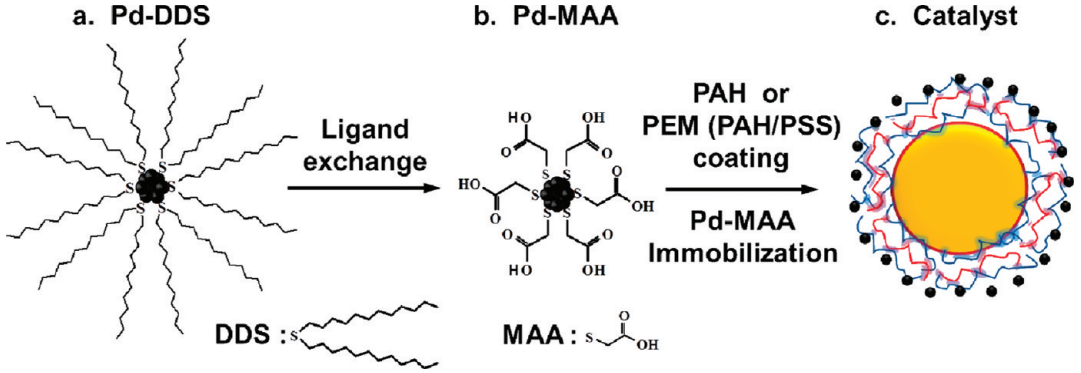

throughout the entire thin film of PEMs. The "encapsulated" nature of the Pd nanoparticles may result in a decreased utilization efficiency of the metal and therefore lead to decreased productivity of the catalyst.

Herein, we present a highly efficient and industrially relevant catalyst design for the direct synthesis of H_2O_2 from H_2 and O_2. The new catalyst is prepared through the stable immobilization of ready-made Pd nanoparticles onto the outermost surface of sulfonated polystyrene resin coated with a positively charged polymer. The Pd nanoparticles are deposited at the periphery of the catalyst such that most of the active sites are always exposed to the reaction mixture and are easily accessible to migrating reactants. In addition, the use of polyelectrolyte enables the highly stable anchoring of nanoparticles onto the support. These characteristic features, or a combination of these advantages, may satisfy most of the requirements for the commercial application of hydrogen peroxide synthesis from hydrogen and oxygen.

The preparation of the catalyst is summarized in Scheme 1. We first synthesize monodispersed Pd nanoparticles through the thermal decomposition of palladium acetate in the presence of dodecyl sulfide (DDS) as a ligand to prevent aggregation of the nanoparticles. The one-step pyrolysis procedure is typically performed in toluene at 95 °C for 1 h. After the decomposition and reduction of the palladium acetate, the color of the reaction medium turns from yellow to black, which indicates the successful formation of colloidal Pd nanoparticles. For the efficient anchoring of the Pd nanoparticles onto sulfonated polystyrene (PS) resin (K2621, Lewatit (Bayer AG), Leverkusen, North Rhine-Westphalia, Germany), the hydrophobic DDS ligand of the Pd nanoparticles is exchanged with the water-soluble ligand mercaptoacetic acid (MAA). The surface of the sulfonated PS resin is also decorated with positively charged poly(allylamine hydrochloride) (PAH) or alternating stacking of PAH and negatively charged polystyrene sulfonate (PSS). Thus, the negatively charged MAA can easily interact with positively charged PAH through an electrostatic interaction force in aqueous solutions.

RESULTS AND DISCUSSION

TEM and XRD Analysis for Characterization of Pd Nanoparticles and Immobilized Pd Nanoparticles. The synthetically prepared Pd nanoparticles are examined using transmission electron microscopy (TEM) and X-ray diffraction (XRD) for the analysis of size, interplanar spacing, monodispersity, and crystallinity (Figure 1). Particle size distributions of the Pd nanoparticles show high monodispersity with low variation (0.2 nm) (Figure 1a,d), which confirms that the synthesis-and-modification route is efficient for the production of uniform Pd nanoparticles, although no size-selective process is performed. The interplanar spacing of the highly crystalline synthetic Pd-DDS nanoparticles is 0.23 nm, which agrees well with the (111) lattice plane of face-centered cubic (fcc) Pd metal (Figure 1b).[20]

The electron diffraction patterns of the Pd-DDS particles show four sharp diffused rings, which are assigned to the diffractions from the (111), (200), (220), and (311) planes of a fcc Pd phase, as shown in Figure 1c. The X-ray diffraction (XRD) pattern of the Pd-DDS particles also shows the characteristic peaks of a fcc structure (Figure 1g). In addition, the crystal size of the Pd samples calculated from the line broadening of the (111) reflection using the Scherrer formula[21] is 2 nm, in good agreement with the size of the particles (2.3 nm) as shown in Figure 1b. After the hydrophobic DDS ligands of the Pd nanoparticles are exchanged with water-soluble ligands (MAA), the HRTEM images, XRD pattern, and electron diffraction pattern of the Pd-MAA samples (Figure 1d, e, f, and g) show an unclear lattice edge, distortion of the domain boundary, and blurred rings, which indicates that the atoms in the crystalline particles are not perfectly stacked. The observed crystallinity change on ligand exchange between DDS and MAA seems to indicate that the chemical nature of the ligand has effect on the Pd nanoparticle structure and crystallinity.[22−24] While detailed mechanism remains elusive, MAA is essential for attaining the change of Pd nanoparticle's crystallinity in solution. As shown in Figure 1a, the Pd nanoparticles show significant volume changes during the ligand exchange, with increase of 200% from Pd-DDS (2.3 nm diameter) to Pd-MAA (2.9 nm diameter) nanoparticles. Thus, the substantial volumetric expansion cause the imperfect stacking of the atoms in the crystalline particles and a large number of defects such as vacancy in the particles, which might be essential for changing the crystallinity of Pd nanoparticles. On the basis of this evidence, it is reasonable to conclude that most of the Pd-MAA particles are amorphous.

With regard to the stability of the catalyst to metal leaching, our previous catalyst design may offer strong advantages because the nanoparticles tend not to escape from the ionically cross-linked architecture of PEMs. The Pd nanoparticles closely encapsulated in an entire thin film, however, may be unfavorable for migrating reactants to access the active sites. The catalytic activity of Pd nanoparticles embedded in a thin charged film can be decreased because of diffusion limitations

dx.doi.org/10.1021/cs300090h | ACS Catal. 2012, 2, 1042−1048

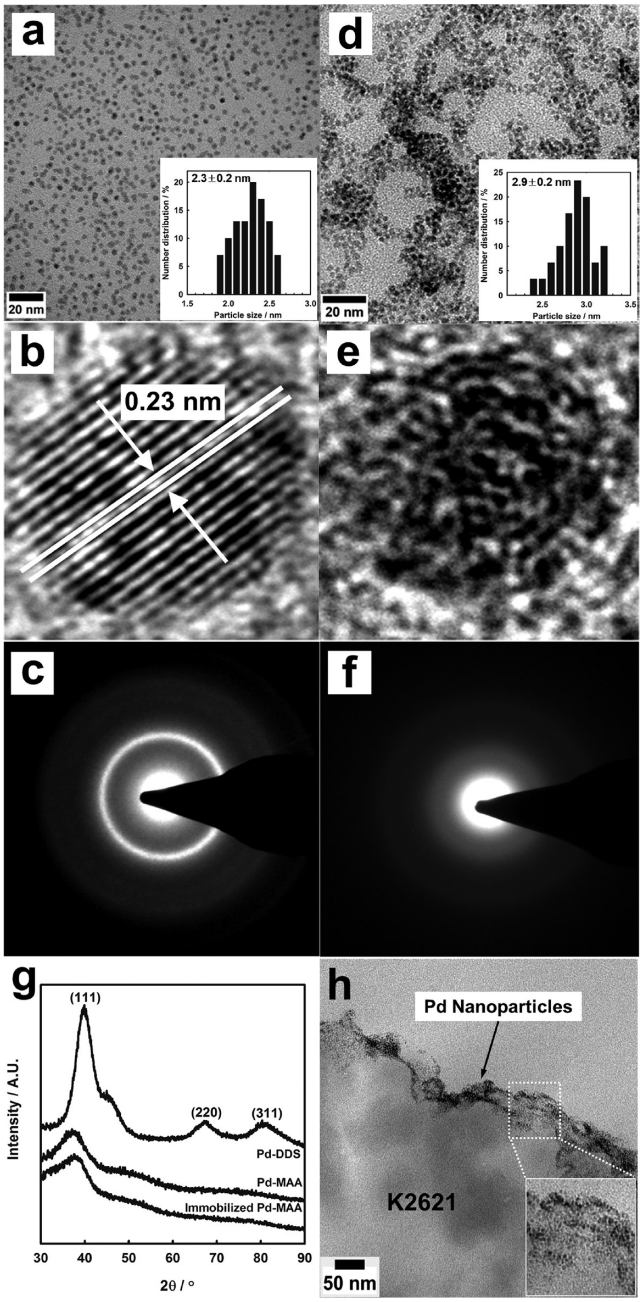

Figure 1. TEM images of (a) Pd-DDS and (d) Pd-MAA nanoparticles; the insets indicate the size distribution. The average particle size and distribution of Pd nanoparticles are determined using the ImageJ software program. Magnified HRTEM images of (b) Pd-DDS and (e) Pd-MAA nanoparticles. Electron diffraction patterns of (c) Pd-DDS and (f) Pd-MAA nanoparticles. (g) X-ray diffraction patterns of Pd-DDS and Pd-MAA. (h) Cryo-TEM image of Pd-MAA nanoparticles immobilized onto PAH coated on sulfonated resin.

or the mass transfer of reactants from the reaction medium.[25−29] In this regard, the anchoring of the nanoparticles onto the outermost surface of the support is a more favorable immobilization method.[30] For the efficient immobilization of negatively charged Pd-MAA onto the surface of the support, the outermost surface of the sulfonated resin is tailored with positively charged PAH polymer. The Pd-MAA is subsequently easily anchored onto the PAH-decorated sulfonated resin by electrostatic interactions. After immobilization of the Pd nanoparticles, cryo-TEM analysis is performed without any separation or washing processes, which clearly demonstrates that the particles are uniformly distributed (Figure 1h). The anchoring position indicates that the Pd nanoparticles are properly immobilized onto only the outersurface of the PS resin. Furthermore, no surface aggregation of the Pd nanoparticles is observed, and no nanoparticles are contained in the core region of the resin. The anchored Pd nanoparticles are well distributed and exist as particulates, although polymeric macroporous resins can shrink during the drying process. This arrangement confirms the efficient immobilization of Pd nanoparticles onto the surface of the resin (Figure 1h). These results indicate that the beneficial effect of electrostatic interactions among the negatively charged sulfonated resin, the polyelectrolyte, and the negatively charged Pd nanoparticles results in Pd nanoparticles that are well dispersed across the sulfonated resin.

Furthermore, the architectures of Pd nanoparticles on thin films are more extensively developed by the alternating deposition of cationic PAH and anionic poly(styrene sulfonate) (PSS) onto a sulfonated resin when the uppermost layer of the PAH provides a positively charged surface for the subsequent self-assembly of the Pd-MAA nanoparticles. The immobilization of the nanoparticles onto the functionalized resin strongly depends on the number of polyelectrolyte layers (Figure 2a).

Interestingly, the immobilization yield of the Pd nanoparticles has decreased as the number of deposited layers is increased. Although the differences in immobilization yield of the Pd nanoparticles at each modified layer are difficult to explain completely, the tendency of the yields to decrease may be attributable to an increase in the repulsive force due to the increased number of free negatively charged sulfonate groups in PSS relative to the increased number of layers. The loading amount at a monolayer of the PAH coating corresponded to a maximum immobilization yield of 91%, which indicates that the immobilization method is highly efficient for the preparation of supported Pd nanocatalysts (Figure 2a).

XPS measurements are performed on the Pd-DDS (crystalline nanoparticles), the Pd-MAA (amorphous nanoparticles), and the immobilized Pd-MAA at different layers of the polymeric thin film (Figure 2b,c; Figure S1, Supporting Information). Overall, the XPS spectra of the two kinds of particles (free Pd-DDS/Pd-MAA and the immobilized samples) show distinctive peaks (Figure 2b,c; Figure S1, Supporting Information). In general, the reduced Pd peaks for the $Pd(3d_{5/2})$ and $Pd(3d_{3/2})$ spin−orbit doublet occur at approximately 335 and 340 eV, respectively.[27,31] The XPS spectra of the free Pd-DDS and Pd-MAA nanoparticles indicate that the samples contain metallic Pd. After the Pd-MAA nanoparticles are immobilized onto the sulfonated resin with different numbers of coating layers, the XPS spectra showed binding energies of 337 and 342 eV, which correspond to Pd^{II}. In addition, the spectra collected before and after the immobilization indicate that most of the Pd nanoparticles are oxidized from Pd^0 to Pd^{II} upon immobilization and that the Pd^{II} state is retained, irrespective of the involvement of the reaction (Figures 2b,c). Furthermore, S 2p XPS data show that the reduction of Pd might result from the oxidation of sulfur in the ligand during the immobilization of Pd-MAA onto PAH-K2621 (Figure S1, Table S1, Supporting Information).

Examination of Catalytic Activities for the Direct Synthesis of Hydrogen Peroxide. To evaluate the catalytic performance for the DSHP reaction, various catalysts are examined under intrinsically safe and less-corrosive reaction

dx.doi.org/10.1021/cs300090h | ACS Catal. 2012, 2, 1042−1048

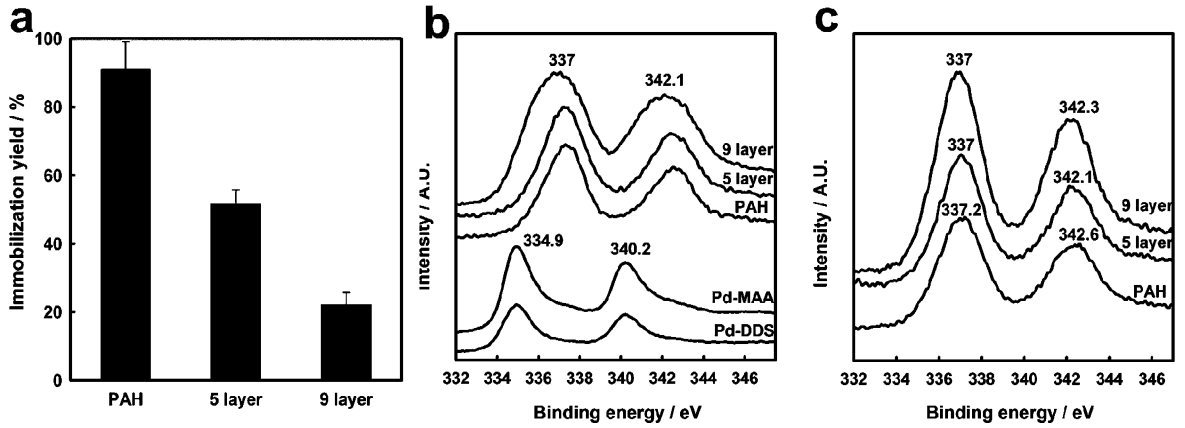

Figure 2. (a) Effect of the number of PEL layers on the immobilization efficiency of Pd-MAA on sulfonated resin, and the XPS spectra of the Pd 3d region of catalysts (b) before and (c) after the reaction.

Table 1. Catalytic Activities of Supported Pd Nanocatalysts for the Direct Synthesis of H_2O_2 from H_2 and O_2[a]

entry	catalyst	Pd (wt%)	TOS (h)	H_2O_2 conc (wt %)	H_2 conv (%)	H_2 selectivity (%)	productivity (g of H_2O_2 (g of Pd)$^{-1}$ h^{-1})
1	Pd/PAH-K2621	0.24	100	8.9	80	73	180
2	PEM^7(Pd)/K2621[b]	0.49	100	7.7	69	73	32
3	Pd/PEM^5-K2621[c]	0.14	100	1.8	58	19	14
4	Pd/PEM^9-K2621[d]	0.06	100	0.2	45	13	5
5	Pd^{II}/K2621[e]	0.72	50	6.1	65	60	17

[a]Reaction conditions: catalyst loading 20 cc; $N_2/H_2/O_2$ (vol %) = 50/3/47 (50 bar); total gas flow rate = 800 mL min^{-1}; liquid flow rate = 0.25 mL min^{-1}; gas/liquid rate ratio = 3200; methanol solvent (1.47×10^{-4} M HBr); 30 °C. [b]Reference 19. [c]Five layers of PEM (PAH/PSS). [d]Nine layers of PEM (PAH/PSS). [e]Commercial Pd-doped sulfonated resin (K2635, Lanxess).

conditions (Table 1). The reaction performance of each catalyst is significantly changed by the characteristics of the applied catalyst, and it is clear that the use of the PAH linker for the immobilization of the palladium nanoparticles is advantageous for the preparation of an efficient catalyst to promote the DSHP reaction (entry 1). The productivity (180 g of H_2O_2 (g of Pd)$^{-1}$ h^{-1}) of the Pd/PAH-K2621 catalyst confirms its high catalytic activity, and the produced H_2O_2 concentration (8.9 wt %) is sufficient to satisfy the previously discussed industrial target. Compared with our previous catalyst design based on the encapsulation of Pd nanoparticles in PEMs (entry 2), the Pd/PAH-K2621 catalyst shows an obvious improvement in H_2O_2 concentration and H_2 conversion. In particular, the H_2O_2 productivity of the new catalyst (entry 1) is six times higher than that of the previous catalyst (entry 2), and the high production of H_2O_2 implies that the utilization efficiency of the active sites in the catalysts can be greatly enhanced by the arrangement of Pd nanoparticles at the periphery, where the reactant mixture can more easily access the active sites. In the case of the Pd nanoparticles encapsulated in PEMs (entry 2), large amounts of Pd nanoparticles exist throughout the electrostatically cross-linked architecture of the PEM thin films. The closely packed or intercalated nature of the Pd nanoparticles may be unfavorable for the accessibility of the active sites and thus lead to a decrease in the efficiency of the catalyst. The Pd catalysts encapsulated in the PEMs therefore result in a sharp decrease in the production of H_2O_2, although a large amount of Pd nanoparticles (0.49 wt %) is loaded and exists at the external surface of the support. In the case of the use of PEMs as a linker, the poor catalytic performances are attributed to the dramatic decrease in both H_2 conversion and selectivity (entries 3 and 4). In addition, an increase in the number of PEM layers from 5 to 9 also led to a further reduction in the immobilization yield of the Pd nanoparticles. The observed trend in the reaction performances with regard to the applied linkers is consistent with the immobilization efficiency of the Pd nanoparticles onto the support.

Considering that the presence of a large amount of sulfonate groups in the macroporous resin matrix may significantly influence the pH of the reaction medium, the catalytic activity is expected to be strongly affected by the macroenvironment. However, the change in the reaction performance with respect to the immobilization linkers clearly suggests that elegant control of microenvironment of the catalyst, especially around nanoparticles, is critical to the elucidation of a salient design for an efficient catalyst for the DSHP reaction. In this study, the use of the PAH linker is highly favorable compared with stacking of the PEMs on a sulfonated resin by the alternating adsorption of polycationic and polyanionic polyelectrolytes. However, the stacking of PEMs on the support is not always detrimental to the reaction because palladium nanoparticles encapsulated in the closely packed PAH/PSS multilayer exhibit reasonably good catalytic activity (entry 2). Although it is difficult to explain the differences in the reaction performance of PEM-applied catalysts at this stage, the minute change of the environment around the Pd nanoparticles by PEMs may be closely related to the catalytic activity. The commercially available Pd-doped sulfonated resin catalyst shows a poor H_2O_2 production as low as 17 g of H_2O_2 (g of Pd)$^{-1}$ h^{-1}, which is approximately one-tenth that of Pd/PAH-K2621 (entry 5). The poor H_2O_2 production implies not only that the accessibility from the reaction medium toward active sites of the Pd catalysts in the resin matrix is limited but also that relatively larger and irregular Pd particle sizes may result in reduced reaction performance, although the amount of Pd doping is greater than that of other catalysts. These facts suggest that fine

dx.doi.org/10.1021/cs300090h | ACS Catal. 2012, 2, 1042−1048

control of the microenvironment with the selection of a suitable linker, the arrangement of the active sites at the external surface, or a combination of these factors is important to realize an efficient and industrially relevant catalyst design.

Investigation of Decomposition of Hydrogen Peroxide. One of the critical challenges in DSHP reaction is the control of byproduct formation pathways because the Pd catalysts promote both the production and the decomposition of H_2O_2. Therefore, minimizing the H_2O_2 decomposition is a prerequisite to achieving a high yield of H_2O_2. In this respect, the investigation of H_2O_2 decomposition by various catalysts is performed under similar reaction conditions. Interestingly, H_2O_2 decomposition is also remarkably dependent upon the immobilization method, as observed in both the nanoparticle immobilization efficiency and the reaction performance, as shown in Figure 3. Whereas almost no H_2O_2 decomposition occurred without the catalyst, a small amount of H_2O_2 decomposed in the presence of the sulfonated resin (K2621). When PAH or PEMs are used as immobilization linkers in the catalysts, the decomposition rates of H_2O_2 were accelerated as the number of PEM layers was increased.

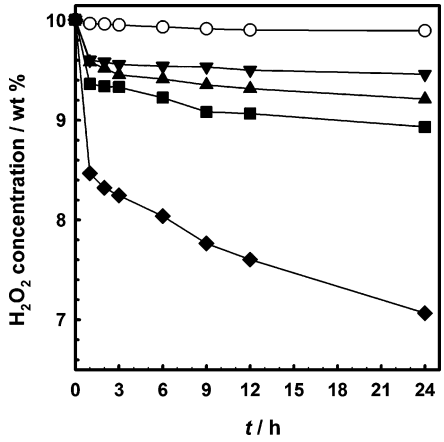

Figure 3. Investigation of H_2O_2 decomposition over various catalysts: natural decomposition (○), K2621 (▼), Pd/PAH-K2621 (▲), Pd/PEM5-K2621 (■), and Pd/PEM9-K2621 (◆). The reaction is performed using H_2O_2 decomposition reaction medium (10 wt % H_2O_2, 1.47×10^{-4} M HBr in MeOH) in a shaking incubator (300 rpm) at a reaction temperature of 30 °C with Pd 0.6 mg/mL (Pd amount/reaction volume).

Indeed, the reaction performance strongly depends on the immobilization methods under real reaction conditions. Although it is difficult to directly relate the order of H_2O_2 decomposition with the catalytic activity, compared with the sulfonated resin itself, the high yield of H_2O_2 and the productivity of the Pd/PAH-K2621 catalyst indicate that the decomposition of the produced H_2O_2 to H_2O is not significant to reduce the catalytic performance. In the case of the Pd/PEM-K2621 catalysts, a relatively faster decomposition rate of H_2O_2, combined with low H_2 conversion, has resulted in poor reaction performance. These results show that the immobilization method closely affects the decomposition rate of H_2O_2 and consequently exhibits a strong influence on both the H_2 selectivity and the H_2O_2 production.

In addition to the excellent catalytic performance, industrially available catalysts should have strong resistance against leaching from the support. To confirm the stability of the catalysts, we performed leaching tests in the reaction medium (methanol that contained 1.47×10^{-4} M HBr) at room temperature for 24 h. In the case of commercial Pd-doped resins (K2635; Pd^{II}/K2621), the leaching of palladium from the K2635 is obvious because a color change is observed after 1 day (Figure 4). This result indicates that hydrogen peroxide, which is a strong oxidizer, attacks the resin matrix and results in the breakdown of the cross-linked matrix.[32] ICP analysis showed that the total concentration of Pd in the solution is approximately 0.45 wt %, which reveals that 37.5% of the palladium was eroded from the K2635 support after only 24 h. However, the Pd/PAH-K2621 catalyst exhibits no color changes, and no palladium is detected in the analysis of the resulting liquid, which indicates that the Pd/PAH-K2621 catalyst is highly stable under the reaction conditions. This result is consistent with that of the real reaction-product analysis. The "leach-proof" nature is undoubtedly advantageous because the resulting nonacidic and metal-free H_2O_2/methanol solution can be directly used as an oxidant in an oxidation reaction, for example, propylene epoxidation, without unfavorable neutralization, purification, or concentration processes; these advantages greatly improve the efficiency and cost-effectiveness of the entire process.[33]

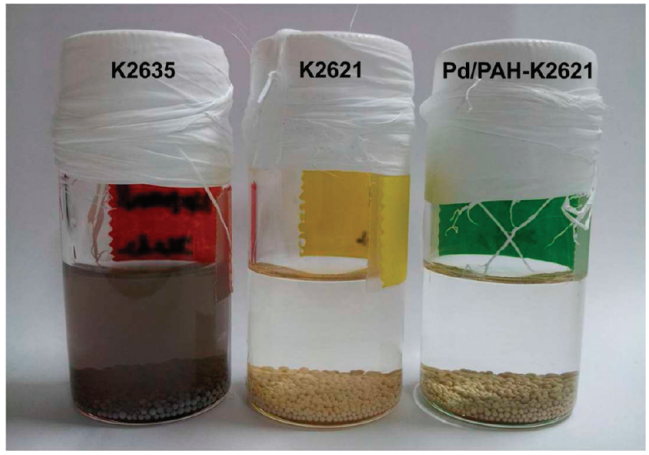

Figure 4. Images of Pd leaching from commercial Pd-doped K2635, K2621, and Pd/PAH-K2621. The catalysts are examined in the reaction medium (MeOH containing 1.47×10^{-4} M HBr) at 30 °C for 24 h.

CONCLUSION

In summary, we have presented the successful development of a highly efficient and industrially relevant catalyst for the direct synthesis of hydrogen peroxide from hydrogen and oxygen. The unique catalyst design, including the arrangement of Pd nanoparticles at the periphery of the support, the use of a PAH linker, and the use of sulfonated resin, makes it possible, for the first time, to meet industrial targets under intrinsically safe and less-corrosive conditions without any loss of activity throughout the course of the reaction. The immobilization efficiency of the nanoparticles on the outermost surface, as well as the reaction performance and "leach-proof" stability of the catalysts, are remarkably dependent upon the linker between the macroporous resin matrix and the Pd nanoparticles. This fact suggests that the favorable tuning of the microenvironment induced by the use of an appropriate linker is a critical factor for the catalyst design. A detailed linker screening and a study of the microenvironment and its detailed control are currently in progress.

dx.doi.org/10.1021/cs300090h | ACS Catal. 2012, 2, 1042−1048

EXPERIMENTAL SECTION

Materials. Palladium(Pd) acetate ($Pd(OAc)_2$), *n*-dodecyl sulfide (DDS), mercaptoacetic acid (MAA), toluene, poly(allylamine hydrochloride) (PAH, M_w 56 000), poly(4-styrenesulfonate, ammonium salt) (PSS, M_w 70 000), cerium(IV) sulfate standard solution (0.25 N in 1−4 N sulfuric acid), and ferroin indicator (0.1 wt % solution in water) were purchased from Sigma-Aldrich and used without further purification. Polystyrene resin (K2621 (SO_3^-)) and K2635 (Pd-doped K2621) were kindly provided by Lanxess.

HRTEM and Cryo-TEM. Analysis of high-resolution transmission electron microscopy (HRTEM) was performed using a transmission electron microscope (Philips, Tecnai(FEI), F20, Hillsboro, OR, USA). The TEM samples were prepared by placing one drop of the Pd dispersion onto a holey-carbon-film-coated 400 mesh copper grid. To demonstrate the proper immobilization and uniformly distributed Pd nanoparticles on the functionalized PS resin, cryo-TEM (JEOL-JEM 2100F FE-TEM, JEOL Ltd., Tokyo, Japan) was used. The specimens were prepared by cryogenic microtoming after high-pressure freezing of the catalyst.

XRD and XPS Analyses. X-ray diffraction measurements were performed on a Bruker-AXS D8 Advance instrument (Karlsruhe, bundesland, Germany) equipped with a Cu Kα radiation (λ = 1.5406 Å) source. Binding energies of Pd in the catalyst were measured using XPS (MultiLab 2000, MultiLab 2000, Thermo VG Scientific, UK, England). Data were acquired with a pass energy of 50 eV, a step increment of 1 eV, and an Al anode. XPS peak positions are referenced to the carbon (1 s) peak at 284.6 eV.

ICP Analysis. Pd content and immobilization yield were obtained by ICP-AES analysis using a Perkin-Elmer OPTIMA 3300 DV (Norwalk, CT, USA).

Synthesis of Pd Nanoparticle. Monodisperse Pd nanoparticles (Pd-DDS) were synthesized using the procedure reported by Obare et al.[34] Briefly, palladium acetate (0.60 g, 2.63 mmol) and *n*-dodecyl sulfide (4.88 g, 13.15 mmol) were added to 50 mL of toluene. The resulting solution was heated to 95 °C with vigorous stirring under a N_2 atmosphere and aged at this temperature for 1 h. The solvent was removed under vacuum, and the Pd nanoparticles were redispersed in acetone. The excess DDS ligand was removed by three repeated cycles of centrifugation (20 000 × *g*), washing with acetone, and redispersion. Finally, the Pd nanoparticles were redispersed in toluene (50 mL).

Ligand Exchange of Pd-DDS with MAA. The ligand exchange of *n*-dodecyl sulfide (DDS) with mercaptoacetic acid (MAA) was performed based on the method of Nie and Chan.[35] Briefly, MAA (13.35 mmol, 912 μL) was added into the Pd nanoparticles (Pd-DDS). This mixture was heated to 60 °C and stirred for 12 h The residual DDS in the MAA-substituted Pd nanoparticle dispersion was removed by three repeated cycles of centrifugation (20 000 × *g*), washing with toluene, and redispersion in DI water. For further purification, the Pd-MAA dispersion was filtered with a centrifugal concentrator (Vivaspin 20(5kD); polyethersulfone membranes; VWR International Ltd., Leicestershire, England) by centrifugation. Finally, the Pd-MAA dispersion was adjusted to pH 6 with 0.1 M HCl or 0.1 M NaOH.

Polyelectrolyte (PEL) Coating on Polystyrene (PS) Resin. PAH solution was prepared at 2×10^{-2} M (based on the repeat-unit molecular weight), and PSS solution was prepared at 6×10^{-2} M individually in DI water and adjusted to pH 9 with 0.1 M HCl or 0.1 M NaOH.

PS resins coated with polyelectrolyte multilayers (PEMs) were prepared by alternate adsorption of PAH (2×10^{-2} M, pH 9) and PSS (6×10^{-2} M, pH 9). PS resin (10 g, dried) was washed three times with DI water. The PEMs were subsequently formed by repeated exposure of the PS resin to PAH and PSS solution for 20 min. In each step, the nonadsorbed PAH and PSS were removed by washing three times with DI water before the next layer was coated. This procedure was repeated until the desired PEMs were formed (PAH, PEM^5, PEM^9) on the PS resin individually. The water used in all experiments exhibits a resistivity greater than 18.2 MΩ·cm and is obtained from a Millipore Mill-Q academic A10 system (Millipore, Bedford, MA, USA).

Pd-MAA Immobilization onto Functionalized PS Resin. The catalyst, Pd-MAA nanoparticles immobilized on the functionalized PS resin, was prepared by electrostatic immobilization. Three milliliters of a Pd-MAA (0.36 wt %) dispersion was added to the three different types of functionalized PS resin (PAH, PEM^5, PEM^9-K2621, prepared using a PEL coating process) for Pd-MAA nanoparticle immobilization by lightly shaking for 24 h. The residue was then removed, and the catalysts were washed five times with DI water. Finally, the three different catalysts (Pd/PAH-K2621, Pd/PEM^5-K2621, Pd/PEM^9-K2621) were obtained.

Investigation of Catalytic Activities for DSHP. Catalytic activity tests were performed in an upflow fixed-bed reactor (10 mm ID × 300 mm L) equipped with cooling jacket. In a typical run, 20 cc of catalyst loaded in a reactor was rinsed with pure methanol for 3 h at 30 °C. After the pressure was increased to 50 bar with nitrogen, methanol feed-in was stopped, and a liquid feed that consisted of methanol mixed with 1.47×10^{-4} M HBr was fed to the reactor at total rate of 15 mL/h. The reaction was started by changing the feed from nitrogen to a gas feed mixture that contained 3% hydrogen, 47% oxygen, and 50% nitrogen.

The gas hourly space velocity (GHSV) of the reactions was 2400 h^{-1}, and the gas-to-liquid ratio was 3200. During a reaction, liquid product and off-gas were periodically withdrawn from the reactor for analyses. The H_2O_2 content was measured by titration using cerium(IV) sulfate standard solution (0.25 N in 1−4 N sulfuric acid) and ferroin indicator (0.1 wt % solution in water). The off-gas was analyzed by gas chromatography for hydrogen concentration.

H_2O_2 Decomposition. The investigation of the retardation of H_2O_2 decomposition using different types of catalysts (Pd/PAH-K2621, Pd/PEM^5-K2621, Pd/PEM^9-K2621) was performed in batch reactors that contained K2621 and three types of catalysts (having identical amounts of Pd) in 10 mL of reaction medium (10 wt % H_2O_2, 1.47×10^{-4} M HBr in MeOH). The reaction was performed with shaking (300 rpm), and the reaction temperature was kept constant (30 °C) in a shaking incubator (VS-8480 SF, Vision Scientific, Co. Ltd., Republic of Korea). The H_2O_2 decomposition was measured as a function of time by titration of the sampled solutions.

ASSOCIATED CONTENT

Supporting Information

Assignment of the different components of the S 2p signal at each Pd particle, change of composition of catalyst before and after DSHP reaction, and sulfur 2p spectra of Pd-DDS, Pd-MAA, and Pd/PAH-K2621. This material is available free of charge via the Internet at http://pubs.acs.org.

AUTHOR INFORMATION

Corresponding Author

*E-mail: rhadum@cnu.ac.kr. Phone: 82-42-821-5896.

Author Contributions

§These authors contributed equally to this work.

Notes

The authors declare no competing financial interest.

ACKNOWLEDGMENTS

This work was financially supported by a grant from the Industrial Source Technology Development Programs (Grant 10033093) of the Ministry of Knowledge Economy (MKE) of Korea and the National Research Foundation of Korea (NRF) Grant funded by the Korea government (MEST) (No. 2011-0017322).

REFERENCES

(1) Henkel, H.; Weber, W. Manufacture of hydrogen peroxide, U.S. Patent 1,108,752, August 25, 1914.
(2) Samanta, C. *Appl. Catal., A* **2008**, *350*, 133−149.
(3) Choudhary, V. R.; Gaikwad, A. G.; Sansare, S. D. *Angew. Chem., Int. Ed.* **2001**, *40*, 1776−1779.
(4) Burch, R.; Ellis, P. R. *Appl. Catal., B* **2003**, *42*, 203−211.
(5) Campos-Martin, J. M.; Blanco-Brieva, G.; Fierro, J. L. G. *Angew. Chem., Int. Ed.* **2006**, *45*, 6962−6984.
(6) Biasi, P.; Menegazzo, F.; Pinna, F.; Eranen, K.; Canu, P.; Salmi, T. O. *Ind. Eng. Chem. Res.* **2010**, *49*, 10627−10632.
(7) Edwards, J. K.; Hutchings, G. J. *Angew. Chem., Int. Ed.* **2008**, *47*, 9192−9198.
(8) Edwards, J. K.; Ntainjua, E.; Carley, A. F.; Herzing, A. A.; Kiely, C. J.; Hutchings, G. J. *Angew. Chem., Int. Ed.* **2009**, *48*, 8512−8515.
(9) Edwards, J. K.; Solsona, B.; N, E. N.; Carley, A. F.; Herzing, A. A.; Kiely, C. J.; Hutchings, G. J. *Science* **2009**, *323*, 1037−1041.
(10) Edwin, N. N.; Piccinini, M.; Pritchard, J. C. A.; Edwards, J. K.; Carley, A. F.; Moulijn, J. A.; Hutchings, G. J. *ChemSusChem* **2009**, *2*, 575−580.
(11) Liu, Q. S.; Bauer, J. C.; Schaak, R. E.; Lunsford, J. H. *Angew. Chem., Int. Ed.* **2008**, *47*, 6221−6224.
(12) Blanco-Brieva, G.; Cano-Serrano, E.; Campos-Martin, J. M.; Fierro, J. L. G. *Chem. Commun.* **2004**, 1184−1185.
(13) Blanco-Brieva, G.; Capel-Sanchez, M. C.; de Frutos, M. P.; Padilla-Polo, A.; Campos-Martin, J. M.; Fierro, J. L. G. *Ind. Eng. Chem. Res.* **2008**, *47*, 8011−8015.
(14) Blanco-Brieva, G.; Escrig, M. P. D; Campos-Martin, J. M.; Fierro, J. L. G. *Green Chem.* **2010**, *12*, 1163−1166.
(15) Brieva, G. B.; Campos-Martin, J. M.; de Frutos, M. P.; Fierro, J. L. G. *Catal. Today* **2010**, *158*, 97−102.
(16) Sun, M.; Zhang, J. Z.; Zhang, Q. H.; Wang, Y.; Wan, H. L. *Chem. Commun.* **2009**, 5174−5176.
(17) Zhou, L.-K. L. B. Catalyst and process for direct catalytic production of hydrogen peroxide, (H_2O_2), U.S. Patent 6,168,775, January 2, 2001.
(18) Zhou, B.; Rueter, M.; Parasher, S. Supported catalysts having a controlled coordination structure and methods for preparing such catalysts, U.S. Patent 7,011,807, March 14, 2006.
(19) Chung, Y. M.; Kwon, Y. T.; Kim, T. J.; Oh, S. H.; Lee, C. S. *Chem. Commun.* **2011**, *47*, 5705−5707.
(20) Liu, Q. S.; Gath, K. K.; Bauer, J. C.; Schaak, R. E.; Lunsford, J. H. *Catal. Lett.* **2009**, *132*, 342−348.
(21) Patterson, A. L. *Phys. Rev.* **1939**, *56*, 978−982.
(22) Liu, Y.; Wang, C.; Wei, Y. J.; Zhu, L. Y.; Li, D. G.; Jiang, J. S.; Markovic, N. M.; Stamenkovic, V. R.; Sun, S. H. *Nano Lett.* **2011**, *11*, 1614−1617.
(23) Wang, C.; Tian, W. D.; Ding, Y.; Ma, Y. Q.; Wang, Z. L.; Markovic, N. M.; Stamenkovic, V. R.; Daimon, H.; Sun, S. H. *J. Am. Chem. Soc.* **2010**, *132*, 6524−6529.
(24) Zhang, H. Z.; Gilbert, B.; Huang, F.; Banfield, J. F. *Nature* **2003**, *424*, 1025−1029.
(25) Niu, Y. H.; Yeung, L. K.; Crooks, R. M. *J. Am. Chem. Soc.* **2001**, *123*, 6840−6846.
(26) Kidambi, S.; Dai, J. H.; Li, J.; Bruening, M. L. *J. Am. Chem. Soc.* **2004**, *126*, 2658−2659.
(27) Kidambi, S.; Bruening, M. L. *Chem. Mater.* **2005**, *17*, 301−307.
(28) Jiang, S. P.; Liu, Z. C.; Tian, Z. Q. *Adv. Mater.* **2006**, *18*, 1068−1072.
(29) Deligoz, H.; Yilmazturk, S.; Karaca, T.; Ozdemir, H.; Koc, S. N.; Oksuzomer, F.; Durmus, A.; Gurkaynak, M. A. *J. Membr. Sci.* **2009**, *326*, 643−649.
(30) Shutava, T. G.; Kommireddy, D. S.; Lvov, Y. M. *J. Am. Chem. Soc.* **2006**, *128*, 9926−9934.
(31) Kumar, G.; Blackburn, J. R.; Albridge, R. G.; Moddeman, W. E.; Jones, M. M. *Inorg. Chem.* **1972**, *11*, 296−300.
(32) Yu, J. R.; Yi, B. L.; Xing, D. M.; Liu, F. Q.; Shao, Z. G.; Fu, Y. Z. *Phys. Chem. Chem. Phys.* **2003**, *5*, 611−615.
(33) Chemsystems PERP Program PERP 07/08-3, Hydrogen Peroxide, 2009, p 47.
(34) Ganesan, M.; Freemantle, R. G.; Obare, S. O. *Chem. Mater.* **2007**, *19*, 3464−3471.
(35) Chan, W. C. W.; Nie, S. M. *Science* **1998**, *281*, 2016−2018.